

See discussions, stats, and author profiles for this publication at: <https://www.researchgate.net/publication/47793015>

What is the Origin of the Prepeak in the X-ray Scattering of Imidazolium-Based Room-Temperature Ionic Liquids?

ARTICLE *in* THE JOURNAL OF PHYSICAL CHEMISTRY B · NOVEMBER 2010

Impact Factor: 3.3 · DOI: 10.1021/jp108545z · Source: PubMed

CITATIONS

126

READS

55

4 AUTHORS, INCLUDING:



Hemant K. Kashyap

Indian Institute of Technology Delhi

26 PUBLICATIONS 650 CITATIONS

[SEE PROFILE](#)



Pablo Martin De Biase

The University of Calgary

18 PUBLICATIONS 395 CITATIONS

[SEE PROFILE](#)

What is the Origin of the Prepeak in the X-ray Scattering of Imidazolium-Based Room-Temperature Ionic Liquids?

Harsha V. R. Annappureddy, Hemant K. Kashyap, Pablo M. De Biase, and Claudio J. Margulis*

Department of Chemistry, University of Iowa, Iowa City, Iowa 52242, United States

Received: September 7, 2010; Revised Manuscript Received: October 11, 2010

The observation of a first sharp diffraction peak (FSDP) at low frequency in the X-ray and neutron scattering spectra of different imidazolium-based room-temperature ionic liquids (RTILs) (the so-called prepeak) has often been experimentally interpreted as indicative of mesoscopic organization leading to nanoscale segregation and the formation of domains of different morphologies. This interpretation that has permeated the analysis of many recently published articles deserves an in depth theoretical analysis. In this article, we use several different computational techniques to thoroughly dissect the atomistic components giving rise to the low-frequency FSDP as well as other features in the structure function ($S(q)$). By understanding how $S(q)$ changes as imidazolium-based ionic systems undergo solid–liquid phase transition, and by artificially perturbing the liquid structure in a way that directly couples to the intensity of the FSDP, we are able to identify in a rigorous way its geometric origin. Similar to the solid phase, the liquid phase is characterized by two typical length scales between polar groups. The shorter length scale gives rise to a shoulder peak in $S(q)$ at about 0.9 \AA^{-1} whereas the longer one gives rise to the prepeak.

1. Introduction

Prepeaks or first sharp diffraction peaks (FSDPs) (in this article these two terms are used interchangeably) are by no means peculiar or exclusive to room-temperature ionic liquids (RTILs), and neither is the controversy on their geometrical origin. X-ray measurements and computer simulations show that common nonionic liquids such as octanol also display a FSDP below 0.5 \AA^{-1} .^{1–3} Whether these features carry relevant information about structure in the liquid phase has been a source of extensive debate in the glass/melt/noncrystalline solid community (see for example citations 4–10 and the many references therein).

In the case of RTILs, pioneering work by Bradley and co-workers¹¹ on long chain 1-alkyl-3-methylimidazolium ($C_n\text{MIM}^+$) systems demonstrated the existence of low-angle FSDPs in the crystalline and liquid crystalline phases that transformed into a broader low intensity peak upon melting (see Figure 2 in ref 11). Early computational work by Urahata and Ribeiro¹² also predicted the occurrence of a prepeak in the Cl^- component of the $S(q)$ in their 1-alkyl-3-methylimidazolium systems. Urahata and co-workers carefully highlighted the standing controversy on the origin of these types of features in the high-temperature ionic melt literature.

Insightful work by Wang and Voth,^{13–15} Bhargava et al.,¹⁶ and Lopez and Padua^{17,18} directed the attention of the RTILs community^{19,20} to the interesting morphology of these systems as observed in computer simulations. It is clear from these authors' early work that because of Coulomb interactions, imidazolium heads and anions associate, and longer cationic alkyl tails appear to aggregate. Approximately at the same time, some very interesting experiments by the group of Triolo^{21–23} showed that the prepeak observed by Bradley and co-workers on imidazolium liquids with very long alkyl tails could also be

detected in systems with cations possessing shorter tails. These experiments greatly enhanced our understanding of the systematic structural and dynamical changes in the prepeak to be expected as the length of the longest cationic alkyl tail is adjusted. To interpret the observed structural dependency of the FSDP on alkyl tail length, different ideas have been proposed. These include cationic tail interdigitation or the formation of micelles (see for example Figure 3 in ref 23), which could account for the alkyl tail length dependence on the q value at which the prepeak shows in Triolo's SAXS experiments. This type of interpretation involving the notion of complex long-range multicenter correlations to form micelles, strands, and other more complex morphologies even in the case of imidazolium systems of modest tail lengths such as $C_5\text{MIM}^+$ has become quite popular (see, for example, refs 24 and 25). However, recent work by Hardacre and co-workers²⁶ has suggested that the prepeak is a simple consequence of cationic anisotropy, which imposes certain patterns of coordination along the direction of the longer alkyl tail and not due to complex long-range morphologies. The current article attempts to combine detailed computer simulations with evidence from published experimental data to clarify the geometrical origin of the prepeak in imidazolium based ILs with spherical or pseudospherical anions. In particular, we will work with the $[C_6\text{MIM}][\text{Cl}]$, $[C_8\text{MIM}][\text{PF}_6]$, and $[C_{10}\text{MIM}][\text{PF}_6]$ ionic systems.

2. Materials and Methods

All molecular dynamics (MD) simulations were carried out with the GROMACS package.^{27,28} We used OPLS-AA parameters²⁹ with partial charges derived from the work of Lopes and Padua.³⁰ For clarity in the exposition of ideas, much of the preliminary work we did trying to understand the prepeak dependence on simulation box size is not shown. It is sufficient to say that if the box length is larger than $2[(2\pi/q_{\text{prepeak}})]$, there is a dependency on the intensity (but not the position) of the

* To whom correspondence should be addressed: E-mail: claudio-margulis@uiowa.edu.

prepeak with box size. Boxes with sides smaller than this threshold value should never be used since obviously they will not display any prepeak. In practice, we find that 300 pairs of ions periodically replicated are adequate to properly account for all features in $S(q)$ above 0.24 \AA^{-1} ; however some of our simulations consisted of up to 21 952 ion pairs to generate the most accurate possible reciprocal space structure function that we could afford.

All simulations involving $[\text{C}_6\text{MIM}][\text{Cl}]$ except for those in Section 3.4 were carried out with 21 952 ion pairs corresponding to 702 464 atoms. Simulations of $[\text{C}_8\text{MIM}][\text{PF}_6]$ were 2744 ion pairs in size whereas in our study of melting of $[\text{C}_{10}\text{MIM}][\text{PF}_6]$ we used 576 ion pairs. Because of the larger computational cost involved in the multivariate global optimization procedure described in Section 3.4, this study was done with an equilibrated simulation box of 300 $[\text{C}_6\text{MIM}][\text{Cl}]$ ion pairs.

Since RTILs are slow dynamical systems, one must be very careful in obtaining thoroughly equilibrated initial conditions suitable for production. We equilibrated each of our systems for several nanoseconds by lowering and raising the value of partial charges (from 0 to 100%) as well as the temperature until volume and structure was converged for the fully charged system at the desired target temperature. The large system with 21 952 ion pairs was built by stacking a subsystem of 2744 equilibrated ion pairs and re-equilibrating for 800 ps. Equilibration and production runs were carried out in the NPT (constant number of particles, pressure, and temperature) ensemble using the Berendsen algorithm and the Leap-Frog integration scheme coded in GROMACS.^{27,28} Production runs for $[\text{C}_6\text{MIM}][\text{Cl}]$ and $[\text{C}_8\text{MIM}][\text{PF}_6]$ were performed at 300 K and 1 atm pressure. We used the Particle Mesh Ewald (PME) algorithm with interpolation order 6 and 0.8 Å grid spacing for proper accounting of long-range electrostatic interactions. Cutoffs for Lennard-Jones and real space part of the Coulombic interactions were set to 15 Å.

Melting of $[\text{C}_{10}\text{MIM}][\text{PF}_6]$ was simulated in a triclinic box of symmetry $P2_1/c$ by imposing a temperature ramp in the range 400 to 600 K at 1 atm on a time scale of 1 ns. Subsequently the system was further simulated at 600 K for 2 ns.

All aspects of the global optimization procedure to enrich real space coordinates in the spatial frequencies of the prepeak are discussed in Section 3.4.

3. Results and Discussion

Imidazolium-based systems with longer alkyl tails and with counterions that are spherically- or pseudospherically symmetric tend to show significant similarities in their intermolecular structure. This can be appreciated by comparing corresponding structure functions $S(q)$ at inverse distances below 2 Å⁻¹. This is exemplified in Figure 1 where we show computationally derived $S(q)$ for $[\text{C}_6\text{MIM}][\text{Cl}]$, $[\text{C}_8\text{MIM}][\text{PF}_6]$, and $[\text{C}_{10}\text{MIM}][\text{PF}_6]$ in the liquid state. Features at q values larger than 2 Å⁻¹ are mostly intramolecular in nature and though fairly easy to assign are not the subject of the current article. Three main features below 2 Å⁻¹ are always observed. The prepeak, below 0.5 Å⁻¹, a shoulder at around 0.9 Å⁻¹, and a major peak at around 1.5 Å⁻¹. It turns out that for imidazolium-based systems with these types of counterions, the FSDP and other intermolecular peaks present in the $S(q)$ of the liquid are also often found in the simulated powder spectrum of the crystal (see, for example, ref 32). It is therefore natural to approach the problem first from the perspective of the crystal since much insight can be gained from interpreting these features in terms of distances between Miller planes.

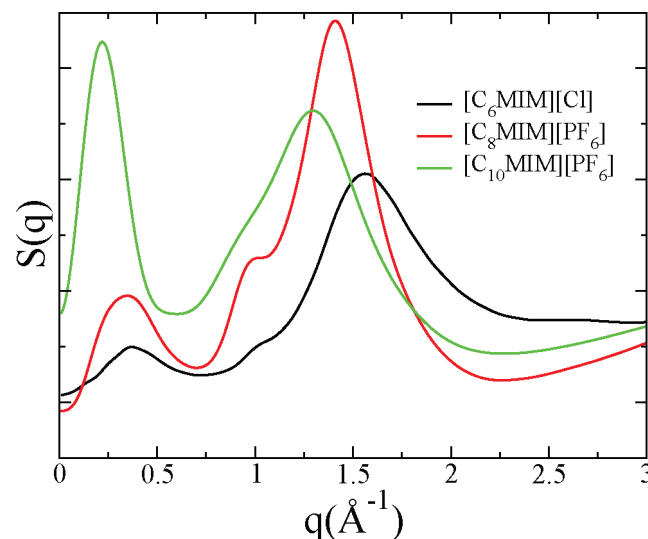


Figure 1. $S(q)$ for liquid $[\text{C}_6\text{MIM}][\text{Cl}]$ and $[\text{C}_8\text{MIM}][\text{PF}_6]$ at 300 K and for $[\text{C}_{10}\text{MIM}][\text{PF}_6]$ at 600 K from our computer simulations described in Section 2.

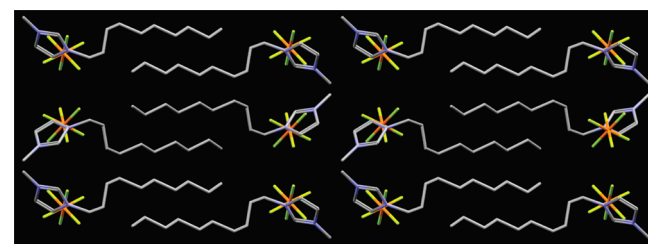


Figure 2. Crystal structure of $[\text{C}_{10}\text{MIM}][\text{PF}_6]$ (identifier ODOLOJ) from ref 31 plotted using the program Mercury.³⁴

3.1. The Prepeak and Other Features of the Crystal.

While imidazolium-based ionic liquids are known to crystallize as different polymorphs,^{32,33} a pattern of anions associated with cationic heads such as that in Figure 2 is quite common.³¹ The asymmetry caused by the longer cationic alkyl tail gives rise to packing patterns with characteristic short and long separations between neighboring polar groups.

From the perspective commonly used in computational theory of liquids, the coherent X-ray intensity ($I_{coh}(q)$) is defined as³⁵

$$S(q) = \frac{I_{coh}(q) - \sum_i x_i f_i^2(q)}{\left[\sum_i x_i f_i(q) \right]^2} \quad (1)$$

In eq 1, i labels an atom type and x_i, f_i are the corresponding atomic fraction and atomic form factor³⁶ of said atom type. Figure 3 shows the coherent intensity computed using eq 1 for $[\text{C}_{10}\text{MIM}][\text{PF}_6]$ crystals of different size constructed by replication of the unit cell³¹ and by applying proper periodic boundary conditions. Since the persistence length scale of a solid is infinite, the peaks converge to δ functions only as the box size approaches the macroscopic limit.

Approaching the same problem from the crystal literature perspective, one can compute the simulated powder pattern coherent intensity³⁴ from the known crystal structure. Each of the lines in the powder spectrum is associated with a family of Bragg crystal planes. Figure 4 shows the coherent intensity computed this way. Clearly, Figures 4 and 3 coincide once broadening is introduced in the powder pattern calculation.

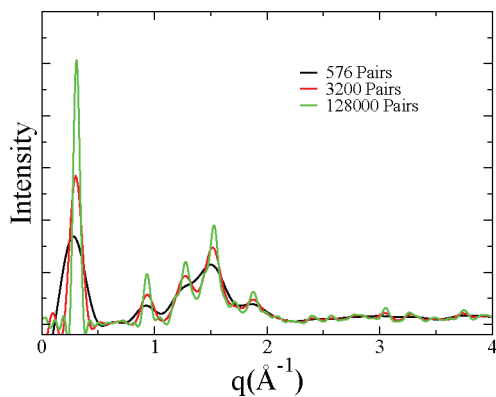


Figure 3. Coherent intensity I_{coh} derived from eq 1 for crystalline $[\text{C}_{10}\text{MIM}][\text{PF}_6]$ as a function of system size computed using proper periodic boundary conditions for space group $P2_1/c$.

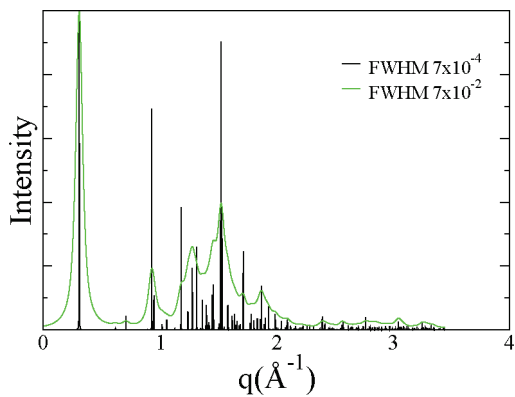


Figure 4. Coherent powder pattern intensity of $[\text{C}_{10}\text{MIM}][\text{PF}_6]$ (identifier ODOLOJ) simulated from the known crystal structure³¹ using Mercury.³⁴ FWHM in units of \AA^{-1} .

The three characteristic features found in the coherent scattering intensity of the liquid (or in $S(q)$) at around 0.4, 0.9, and 1.5\AA^{-1} exist also in the crystal. The single isolated peak in the powder spectrum closest to the frequency of the liquid prepeak corresponds to reflections of the $[1,0,0]$ family of crystal planes. These planes represent the boundary of the unit cell

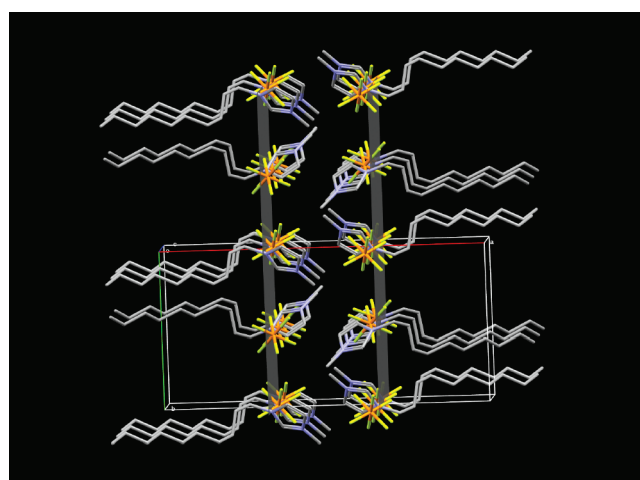


Figure 6. Miller planes $[3,0,0]$ of $[\text{C}_{10}\text{MIM}][\text{PF}_6]$ (identifier ODOLOJ).

perpendicular to the longest cell axis. The shoulder feature in the liquid at about 0.9\AA^{-1} corresponds to the crystal lines at about the same q value that are mainly due to reflections from planes $[3,0,0]$ and $[1,1,-1]$ whereas the intense broad band at around 1.5\AA^{-1} in the liquid corresponds to the scattering of a large number of different crystal planes.

Most scattering intensity in these systems results from the anions and the polar head of the cations (together, commonly referred as the polar groups). It is therefore reasonable to expect Miller planes of high intensity to coincide with loci of high density of polar group scatterers.

Figure 5 shows Miller planes $[1,0,0]$ giving rise to the prepeak in solid $[\text{C}_{10}\text{MIM}][\text{PF}_6]$. Clearly, in the crystal the FSDP corresponds to the typical inverse length separation between polar groups of neighboring ions separated by the longest alkyl tail of the cations.

The intermediate feature at around 0.9\AA^{-1} due to planes $[1,1,-1]$ and $[3,0,0]$ can be interpreted as arising from short characteristic separations between polar groups in adjacent ions not separated by long alkyl tails. Figures 6 and 7 show family of planes $[3,0,0]$ and $[1,1,-1]$ respectively. Within a unit cell,

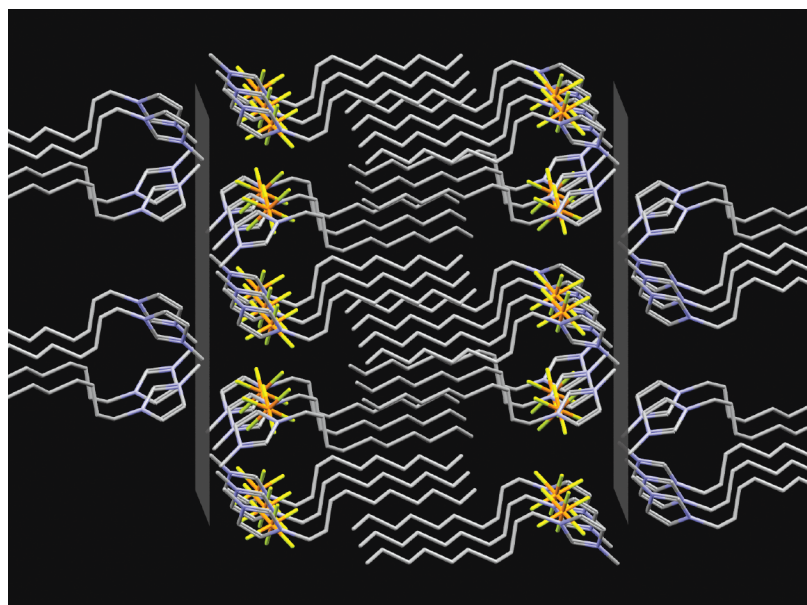


Figure 5. Miller planes $[1,0,0]$ of $[\text{C}_{10}\text{MIM}][\text{PF}_6]$ (identifier ODOLOJ). The scattering from this family of planes gives rise to the prepeak in the solid.

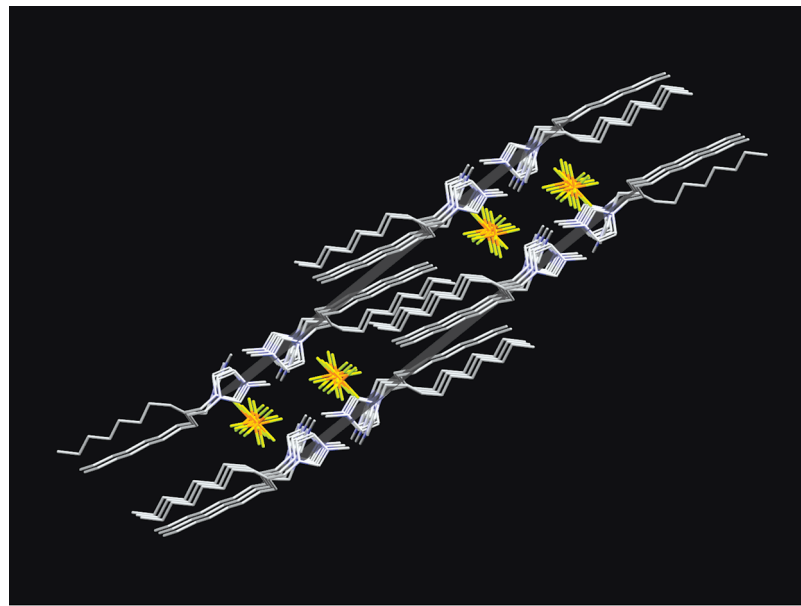


Figure 7. Miller planes [1,1,−1] of $[C_{10}MIM][PF_6]$ (identifier ODOLOJ) that define the characteristic distance between ions of the same charge.

two out of three times planes [3,0,0] fall close to polar groups that are heavily weighted in the coherent intensity by their atomic form factors.

Planes [1,1,−1] are very interesting since they define the characteristic distance between polar groups of the same charge. We will demonstrate in Section 3.3 that our interpretation of this characteristic distance in the solid will still be valid in the liquid for the shoulder peak at around 0.9 \AA^{-1} . Figure 7 shows that [1,1,−1] planes lie almost along the long alkyl tail of the cations and are intercalated by PF_6^- anions. Of the many crystal planes that can be associated with the intense features close to 1.5 \AA^{-1} , those that are intermolecular in nature correspond to short close contact distances between ions.

3.2. The Evolution of the Prepeak and Shoulder Peak Through the Melting Transition and a 3D View of Local Liquid Structure. Figure 8 shows simulated coherent intensity and $S(q)$ for the $[C_{10}MIM][PF_6]$ system as a function of time during melting. As the crystal melts, the change in density results in a shift of all peaks toward lower q values (larger interionic distances). What originally was a peak at around 0.9 \AA^{-1} in the solid phase becomes a shoulder in the liquid phase. The peak originally at about 1.5 \AA^{-1} significantly broadens and shifts to lower q values.

Many of the features in the crystal persist in an average way in the liquid phase. This can be appreciated from the 3D density isosurfaces

depicted in Figure 9a,b around the cations in $[C_6MIM][Cl]$ and $[C_8MIM][PF_6]$, respectively. Figure 9a shows the distribution of Cl^- (red) and C_6MIM^+ heads (green) around C_6MIM^+ whereas Figure 9b shows the distribution of P atoms in PF_6^- (red) and head atoms in C_8MIM^+ (green) around C_8MIM^+ . The alternating nature of the polar components, which for the most part stay away from the nonpolar alkyl tails, is clearly reminiscent of the solid state. A similar analysis can be made from the perspective of the anion. Three-dimensional density isosurfaces of C_8MIM^+ heads and P atoms around PF_6^- in $[C_8MIM][PF_6]$ are shown in Figure 10.

3.3. Which Atomic Correlations Give Rise to the Prepeak and Shoulder Peak in the Liquid Phase? The total static structure function is computed from (eq 2)

$$S(q) = \frac{\rho_0 \sum_i \sum_j x_i x_j f_i(q) f_j(q) \int_0^\infty 4\pi r^2 (g_{ij}(r) - 1) \frac{\sin qr}{qr} dr}{\left[\sum_i x_i f_i(q) \right]^2} \quad (2)$$

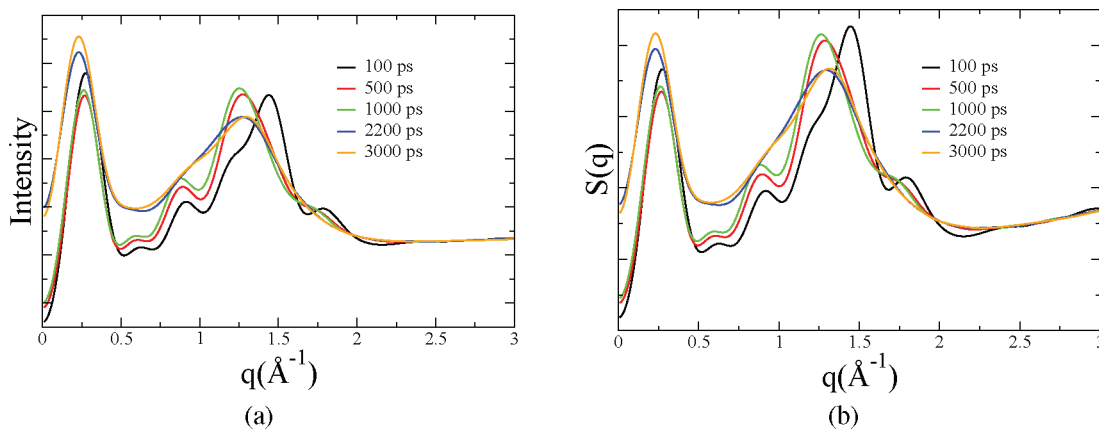


Figure 8. (a) Coherent intensity and (b) $S(q)$ computed along a melting simulation of $[C_{10}MIM][PF_6]$.

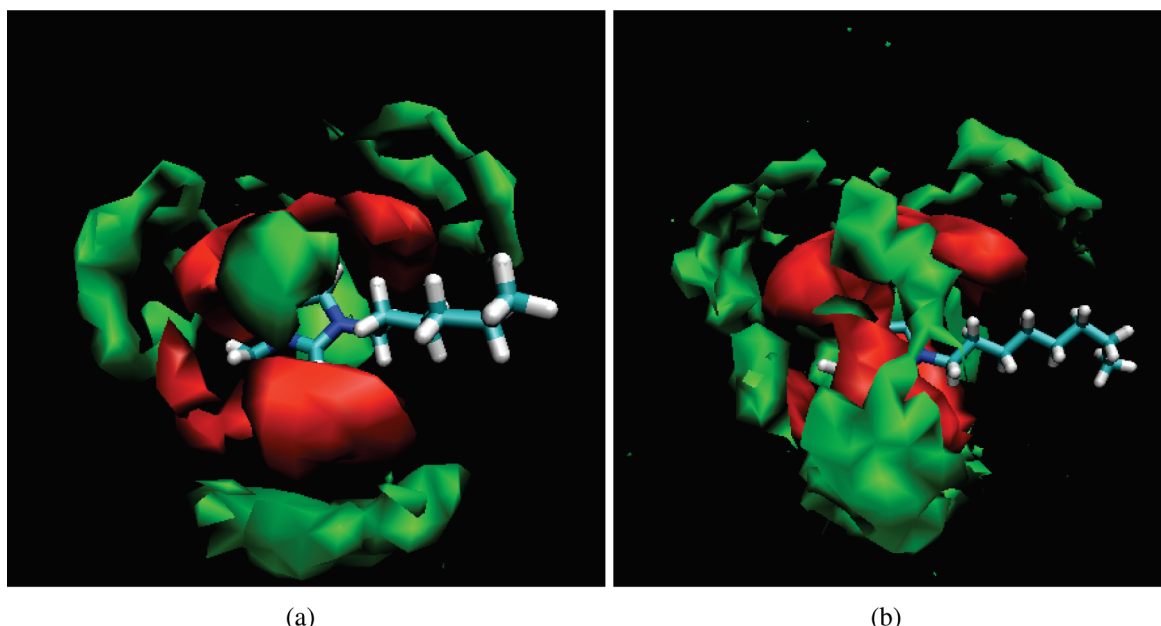


Figure 9. (a) Density isosurfaces of Cl⁻ (red) and C₆MIM⁺ heads (green) around C₆MIM⁺ in [C₆MIM][Cl] and (b) density isosurfaces of P atom in PF₆⁻ (red) and C₈MIM⁺ heads (green) around C₈MIM⁺ in [C₈MIM][PF₆].

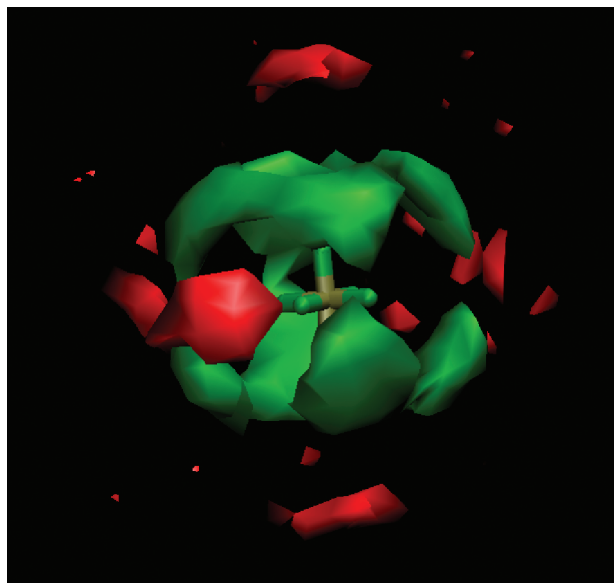


Figure 10. Density isosurfaces of C₈MIM⁺ heads (green) and P atom in PF₆⁻ (red) around PF₆⁻ in [C₈MIM][PF₆].

where, ρ_0 is the bulk density and $g_{ij}(r)$ is the corresponding pair distribution functions for atom types i and j (other quantities have been previously defined in eq 1). To unequivocally identify the species giving rise to the prepeak and shoulder peak, it is instructive to dissect $S(q)$ into its properly form factor weighted subcomponents

$$\frac{\rho_0 x_i x_j f_i(q) f_j(q) \int_0^\infty 4\pi r^2 (g_{ij}(r) - 1) \frac{\sin qr}{qr} dr}{\left[\sum_i x_i f_i(q) \right]^2}$$

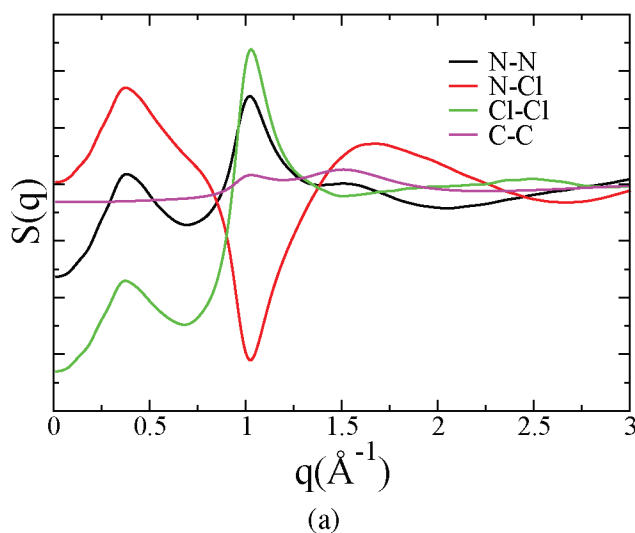
Figure 11a,b shows these subcomponents in the case of [C₆MIM][Cl] and [C₈MIM][PF₆], respectively. It is clear from Figure 11 that in both liquids N atoms and the anion, not the carbons, are responsible for the appearance of the prepeak.

Clearly, just as in the case of solid [C₁₀MIM][PF₆], this indicates that the FSDP is associated with a characteristic inverse length scale between polar groups. This length scale is larger in the liquid since it appears at lower q values as shown in Figure 8. In Section 3.4, we present a detailed analysis of the geometric origin of this characteristic distance in the liquid phase.

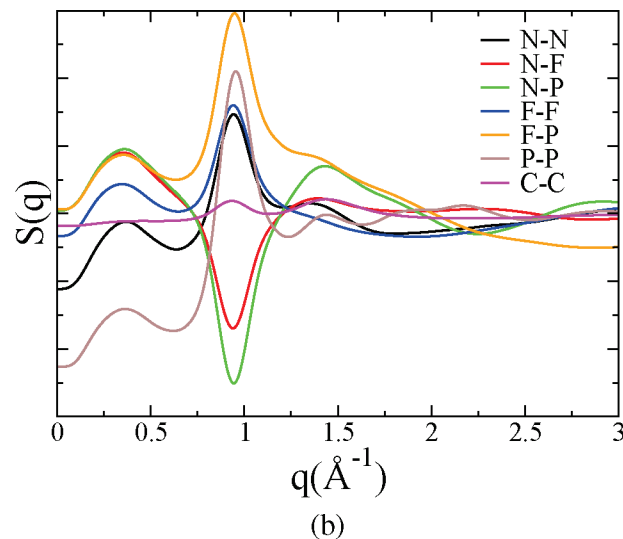
Figure 12 provides complementary information to the selective deuteration neutron scattering studies recently published by Hardacre and co-workers.²⁷ Figure 12 shows why, whereas C and N have similar atomic form factor weights and the fraction of C atoms is much larger, the contribution of C to the prepeak is negligible. Subdividing the carbon contribution into head and tail groups results in the following three terms: Head–Head, Tail–Tail, and Head–Tail. The first two introduce a peak in the $S(q)$ at the prepeak region whereas the cross term introduces a trough that cancels it. This off phase spatial behavior tells us that on average there is absence of tails where one would expect to find heads and vice versa.

This result combined with the fact that in the liquid phase the terminal carbon of the longest alkyl tail is most likely to be found closest to other terminal carbons (as shown in Figure 13) provides some clues regarding the typical separation distance between groups of atoms that without negative interference give rise to the prepeak.

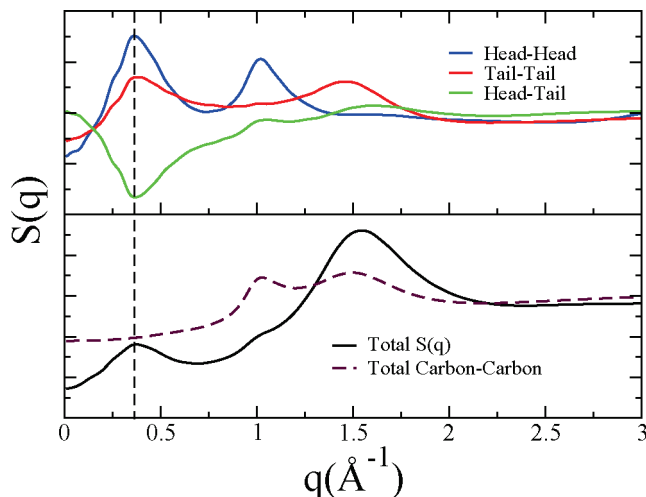
Perhaps equally as interesting in the comparison of solid and liquid phases is the interpretation of the $S(q)$ subcomponents responsible for the shoulder peak at around 0.9 Å⁻¹. In the crystal phase, two planes with Miller indexes [3,0,0] and [1,1,-1] were responsible for this feature (see Figures 6 and 7). Careful mathematical analysis (not shown) explains why in the crystal phase, reflections from the [1,1,-1] planes are of less intensity.^{37,38} The scattering intensity computed from fractional distances and lattice planes turns out to be a sum of cation–cation, anion–anion, and cation–anion cross terms. In the case of the [1,1,-1] plane, all of these terms are large, but the cross term is of similar magnitude and opposite sign resulting in significant intensity cancellation. In Section 3.1, we showed that planes [1,1,-1] define the short interionic distance between polar groups of the same charge (see Figure 7). In the liquid, the feature at 0.9 Å⁻¹ has the same phase characteristics as the



(a)

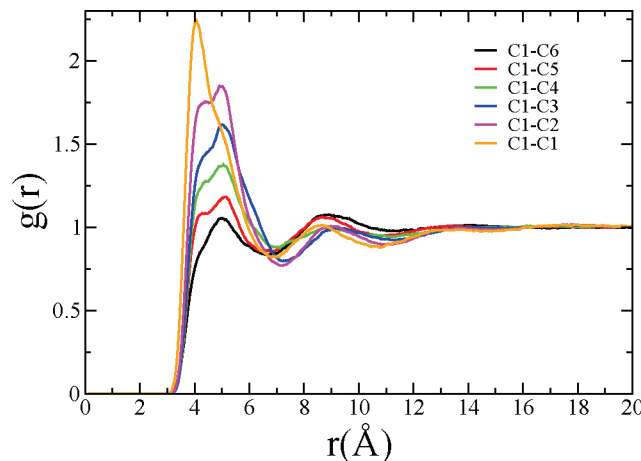


(b)

Figure 11. (a) Atomic subcomponents of $S(q)$ in liquid $[C_6\text{MIM}][\text{Cl}]$ and (b) atomic subcomponents of $S(q)$ in liquid $[C_8\text{MIM}][\text{PF}_6]$.**Figure 12.** Upper panel: Head–Head, Tail–Tail, and Head–Tail partial carbon structure functions of $C_6\text{MIM}^+$ in liquid $[C_6\text{MIM}][\text{Cl}]$. Lower panel: Total $S(q)$ and partial Carbon–Carbon $S(q)$ obtained from the sum of the three functions in the upper panel weighted by $(x_C^{\text{Head}} \times x_C^{\text{Head}})$, $(x_C^{\text{Tail}} \times x_C^{\text{Tail}})$ and $2(x_C^{\text{Head}} \times x_C^{\text{Tail}})$, respectively. Here, $x_C^{\text{Head}} = 4/32$ and $x_C^{\text{Tail}} = 6/32$ are the fraction of head and tail carbon atoms as defined in eq 1. Clearly, there is almost complete cancellation of carbon contribution to the prepeak region.

[1,1,−1] plane in the solid. This is clearly seen from Figure 11a,b where Cl–Cl, P–P, and N–N terms give rise to positive contributions while the cross terms N–Cl or N–P give rise to negative contributions of similar magnitude. This indicates that the periodicity of plane [1,1,−1] is preserved in the liquid phase. Since this length scale corresponds to the short distance between polar groups of the same sign, it can also be interpreted as a periodicity in the absence of ions of opposite charge at that particular distance.

3.4. The Prepeak in the Liquid Phase. An Analysis Solely From the Point of View of the Liquid. While the comparison between liquid and solid spectral features has helped us draw conclusions about the nature of $S(q)$ in the liquid phase, a most satisfying explanation of the origin of the FSDP should be attempted without invoking the now established origin of this feature in the solid. The conclusion of this analysis can at a later point be contrasted against what we know from the crystal phase. Of the different RTILs studied in this article we have chosen to focus in this section on $[C_6\text{MIM}][\text{Cl}]$ because it is

**Figure 13.** Radial distribution function between carbon atoms in the long alkyl tail of $[C_6\text{MIM}][\text{Cl}]$. Carbon atoms are labeled starting at 1 from the terminal carbon.

the shorter alkyl tail systems that challenge our understanding of the identity of the prepeak the most. The prepeak of $[C_6\text{MIM}][\text{Cl}]$ in the liquid state is of low intensity compared to other reciprocal space features in the low q regime. Because in alkylimidazolium systems with shorter tails the inherent disorder in the liquid phase makes it quite difficult to assign longer range correlations unequivocally, to gain important insight, the community has often approached the problem through visual inspection of 3D computer simulation snapshots, that while quite illustrative have the potential to be misleading. This is because snapshots only present circumstantial configurational evidence of structures or morphologies. Instead, we present a method not based on visual inspection that attempts to tease out the global coordinates that couple most strongly to the magnitude of the prepeak.

The inverse Fourier transform of the prepeak corresponds to a real space sum of waves. Since in the liquid state the intensity of the prepeak is small compared to that of other spectral features, filtering out the prepeak in reciprocal space results in real space atomic RDFs with very modest changes. This is evident in the case of the Cl–Cl and Cl–N correlations shown in Figure 14 panels a and b, respectively. The reader is reminded that these are the most important correlations giving rise to the prepeak. One is therefore unable to gain much insight by simple

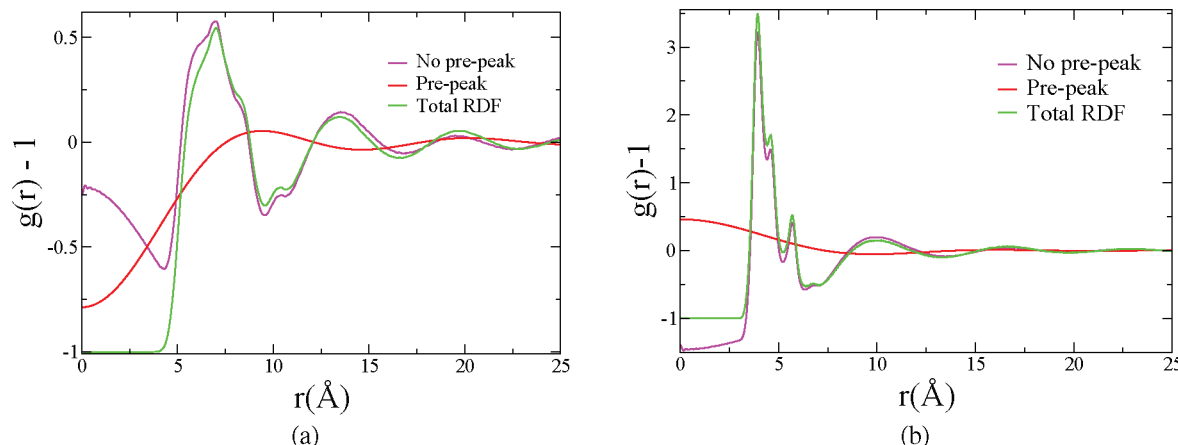


Figure 14. In red is the inverse Fourier transform of the prepeak region; in magenta is ($g(r) - 1$) when the contribution of the prepeak region is filtered out, and in green is the full ($g(r) - 1$) in the case of (a) Cl–Cl correlations and (b) N–Cl correlations in liquid [C₆MIM][Cl]. Clearly filtering out the prepeak produces modest changes in the RDFs of the atomic species that should be the most affected by the prepeak.

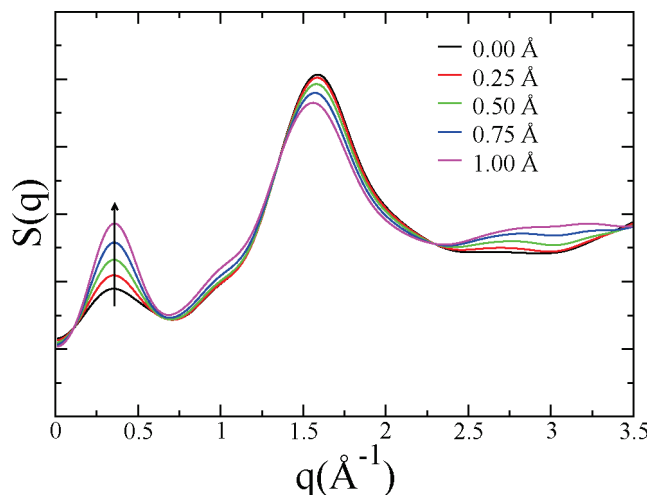


Figure 15. Total $S(q)$ enriched in the frequencies of the prepeak. Ions are displaced along the vector than enhances $S(q)$ in increments defined in the figure legend.

comparison of RDFs that include or exclude information about the prepeak. In other words, geometrically this particular liquid would appear to be quite similar if it had no prepeak. It is therefore our goal to exaggerate this reciprocal space feature as a way to identify its origin in the liquid and to establish global

molecular positions that produce unphysical $S(q)$ s enriched in the frequencies of the prepeak band.

We approach this problem from a multivariate optimization perspective using the praxis algorithm.³⁹ From Figure 11a and eq 2, it is clear that N–N, N–Cl, and Cl–Cl correlations are the most heavily weighted in the prepeak region of liquid [C₆MIM][Cl]. Therefore, the global optimization routine is asked to maximize the intensity of the prepeak generated from the form factor weighted sum of these subcomponents of $S(q)$ by translating ions. We further impose the reasonable geometric constraint that ions not move more than 1 Å. The enrichment of the total $S(q)$ in the frequencies of the prepeak due to this optimization procedure is shown in Figure 15. Figure 16a,b shows RDFs between Cl–Cl and Cl–N as we displace ionic coordinates in the global directions that enrich $S(q)$. The enrichment gives rise to RDFs that clearly show polar groups coming closer together, while the second peak in the RDF becomes of lower intensity and in the case of Cl–Cl slightly moves to longer distances.

Figure 17a shows an enlarged snapshot of the system used for optimization (the actual snapshot is replicated one time in each positive and negative direction along x , y , and z for visual clarity). Figure 17b shows the polar groups in the same liquid snapshot whereas Figure 17c shows the same groups after displacements are applied in the direction derived from the optimization procedure. It is clear that exaggerating the impor-

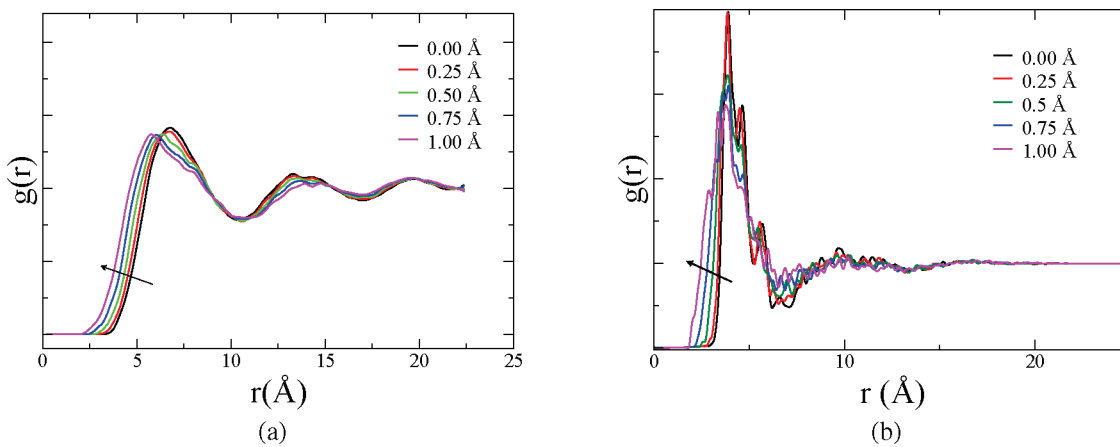


Figure 16. (a) Cl–Cl RDF and (b) N–Cl RDF as global coordinates are displaced to enhance $S(q)$ in the frequencies of the prepeak.

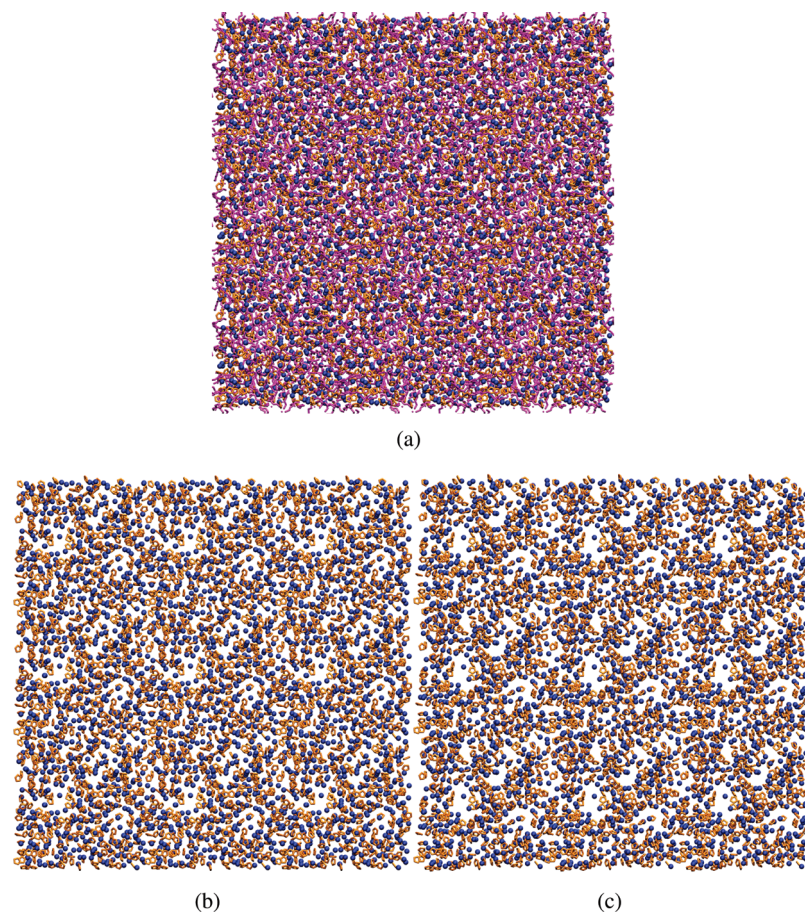


Figure 17. (a) Depicts orthographic view of a typical system snapshot (periodically replicated in $\pm x$, $\pm y$, and $\pm z$); alkyl tails are in magenta, anions in blue and cation heads in orange, (b) shows only cation heads and anions for the same snapshot, while (c) shows the same group of atoms after multivariate optimization to enhance the prepeak.

tance of the prepeak results in the grouping of nearest neighbor polar groups and separation from other polar groups by a characteristic longer length scale.

As shown in Figure 5, in the case of solid $[C_{10}MIM][PF_6]$ this longer length scale is defined by the separation between planes [1,0,0] corresponding to the distance between polar groups separated by the longer cationic alkyl tail. Figure 11a proves that in liquid $[C_6MIM][Cl]$ the mild prepeak also arises due to the correlation between N and Cl atoms. These polar group atoms are separated because of the steric hindrance imposed by the longer cationic alkyl tail. In contrast to what is expected in the solid (as can be seen in the case of $[C_{10}MIM][PF_6]$ in Figure 5), and in agreement with the experiments of Triolo,²³ Figure 13 indicates that in this liquid there is no tail interdigititation.

It is the intrinsic anisotropy in the geometry of the cation along the direction of the longer alkyl tail that prevents the close approach of other polar groups in that particular direction. As a consequence neighboring polar groups can either be in close contact as shown in Figures 9 and 10 or appear further apart if they are separated by the long cationic tail. Since the prepeak is of very low intensity, this anisotropy is only barely noticeable in Figure 17b, however it becomes increasingly visible in Figure 17c as we enhance the coordinates in the frequencies of the prepeak. In brief, both in the liquid and in the solid two characteristic distances exist between adjacent polar groups; a short distance much like the one we would expect from less structured ions giving rise to the shoulder peak at 0.9 \AA^{-1} and a longer separation due to the hindering presence of the long alkyl tail giving rise to the prepeak.

4. Conclusions

Imidazolium-based ionic liquids with moderately long alkyl tails and with spherical or highly symmetrical anions tend to show common features in the low q region of the coherent X-ray scattering intensity. These same features are also often present in the simulated coherent intensity of their solid powder pattern. The broad peak at 1.5 \AA^{-1} is due to intramolecular and close contact intermolecular interactions. Both in the solid and in the liquid phase, the shoulder peak at around 0.9 \AA^{-1} defines the typical short separation distance between polar groups of the same charge. The prepeak in the liquid and strong intensity [1,0,0] Miller planes in the solid define the typical distance between charged groups separated by the long cationic alkyl tails. In this family of systems, the prepeak exists because of the intrinsic anisotropy of the cation. Two kinds of nearest neighbors are possible, those in which close contact between polar groups are sterically allowed and those that because of cationic anisotropy are separated by a typical longer lengthscale associated with the long cationic alkyl tail.

While the existence of complex morphologies is neither proved nor disproved by our study, it is fair to say that the anisotropy in the cation is a necessary but not a sufficient condition for such morphologies. While it is possible that these liquids form such structures as micelles, sheets, and sponges, it would appear that the prepeak can be explained by much simpler consideration of solvation shell asymmetry as has been recently discussed in ref 26. The asymmetry giving rise to the prepeak scales with alkyl tail length since tails are the spacers between

the strongly scattering polar groups. If this is what is meant by micelles, then perhaps much of the controversy is simply semantics!

Acknowledgment. We would like to thank Dr. Dale Swenson for insightful discussions on crystallography. This work was supported by the U.S. Department of Energy, Office of Basic Energy Sciences, Division of Chemical Sciences, Geosciences, and Biosciences under SISGR Grant DE-FG02-09ER16118. This work was originally started with support by the National Science Foundation under CAREER award 0547640. Any opinions, findings, and conclusions or recommendations expressed in this material are those of the author(s) and do not necessarily reflect the views of any funding agency.

References and Notes

- (1) Chen, B.; Siepmann, J. I. *J. Phys. Chem. B* **2006**, *110*, 3555–3563.
- (2) Franks, N. P.; Abraham, M. H.; Lieb, W. R. *J. Pharm. Sci.* **1993**, *82*, 466–470.
- (3) Vahvaselka, K. S.; Serimaa, R.; Torkkeli, M. *J. Appl. Crystallogr.* **1995**, *28*, 189–195.
- (4) Hajdu, F. *J. Non-Cryst. Solids* **2000**, *277*, 15–21.
- (5) Jergel, M.; Mrafko, P. *J. Non-Cryst. Solids* **1986**, *85*, 149–161.
- (6) Price, D. L. *Curr. Opin. Solid State Mater. Sci.* **1996**, *1*, 572–577.
- (7) Bychkov, E.; Benmore, C. J.; Price, D. L. *Phys. Rev. B* **2005**, *72*, 172107.
- (8) Mei, Q.; Benmore, C. J.; Sen, S.; Sharma, R.; Yarger, J. L. *Phys. Rev. B* **2008**, *78*, 144204.
- (9) Wilson, M.; Madden, P. A. *Phys. Rev. Lett.* **1994**, *72*, 3033–3036.
- (10) Soyer Uzun, S.; Sen, S.; Benmore, C. J.; Aitken, B. G. *J. Phys.: Condens. Matter* **2008**, *20*, 335105.
- (11) Bradley, A. E.; Hardacre, C.; Holbrey, J. D.; Johnston, S.; McMath, S. E. J.; Nieuwenhuyzen, M. *Chem. Mater.* **2002**, *14*, 629–635.
- (12) Urahata, S. M.; Ribeiro, M. C. C. *J. Chem. Phys.* **2004**, *120*, 1855–1863.
- (13) Wang, Y.; Jiang, W.; Yan, T.; Voth, G. A. *Acc. Chem. Res.* **2007**, *40*, 1193–1199.
- (14) Wang, Y.; Voth, G. A. *J. Phys. Chem. B* **2006**, *110*, 18601–18608.
- (15) Wang, Y.; Voth, G. A. *J. Am. Chem. Soc.* **2005**, *127*, 12192–12193.
- (16) Bhargava, B. L.; Devane, R.; Klein, M. L.; Balasubramanian, S. *Soft Matter* **2007**, *3*, 1395–1400.
- (17) Canongia Lopes, J. N. A.; Padua, A. A. H. *J. Phys. Chem. B* **2006**, *110*, 3330–3335.
- (18) Gomes, M.; Lopes, J.; Padua, A. *Top. Curr. Chem.* **2009**, *290*, 161–183.
- (19) Wishart, J. *J. Phys. Chem. Lett.* **2010**, *1*, 1629.
- (20) Castner, J. E. W.; Wishart, J. F. *J. Chem. Phys.* **2010**, *132*, 120901–1–20901–9.
- (21) Russina, O.; Triolo, A.; Gontrani, L.; Caminiti, R.; Xiao, D.; Hines, L. G.; Bartsch, R. A.; Quitevis, E. L.; Pleckhova, N.; Seddon, K. R. J. *Phys.: Condens. Matter* **2009**, *21*, 424121.
- (22) Triolo, A.; Russina, O.; Bleif, H.-J.; Di Cola, E. *J. Phys. Chem. B* **2007**, *111*, 4641–4644.
- (23) Triolo, A.; Russina, O.; Fazio, B.; Triolo, R.; DiCola, E. *Chem. Phys. Lett.* **2008**, *457*, 362–365.
- (24) Chiappe, C. *Monatsh. Chem.* **2007**, *138*, 1035–1043.
- (25) Xiao, D.; Rajian, J. R.; Li, S. F.; Bartsch, R. A.; Quitevis, E. L. *J. Phys. Chem. B* **2006**, *110*, 16174–16178.
- (26) Hardacre, C.; Holbrey, J. D.; Mullan, C. L.; Youngs, T. G. A.; Bowron, D. T. *J. Chem. Phys.* **2010**, *133*, 74510–74517.
- (27) Hess, B.; Kutzner, C.; van der Spoel, D.; Lindahl, E. *J. Chem. Theory Comput.* **2008**, *4*, 435–447.
- (28) van der Spoel, D.; Lindahl, E.; Hess, B.; Groenhof, G.; Mark, A.; Berendsen, H. *J. Comput. Chem.* **2005**, *26*, 1701–1718.
- (29) Jorgensen, W. L.; Maxwell, D. S.; Tirado-Rives, J. *J. Am. Chem. Soc.* **1996**, *118*, 11225–11236.
- (30) Lopes, J. N. C.; Deschamps, J.; Padua, A. A. H. *J. Phys. Chem. B* **2004**, *108*, 2038–2047.
- (31) Gordon, C. M.; Holbrey, J. D.; Kennedy, A. R.; Seddon, K. R. J. *Mater. Chem.* **1998**, *8*, 2627–2636.
- (32) Holbrey, J. D.; Reichert, W. M.; Nieuwenhuyzen, M.; Johnston, S.; Seddon, K. R.; Rogers, R. D. *Chem. Commun.* **2003**, 1636–1637.
- (33) Jayaraman, S.; Maginn, E. J. *J. Chem. Phys.* **2007**, *127*, 214504.
- (34) Macrae, C. F.; Edgington, P. R.; McCabe, P.; Pidcock, E.; Shields, G. P.; Taylor, R.; Towler, M.; van de Streek, J. *J. Appl. Crystallogr.* **2006**, *39*, 453–457.
- (35) Keen, D. *J. Appl. Crystallogr.* **2001**, *34*, 172–177.
- (36) *International Tables for Crystallography*; Prince, E., Ed.; International Union of Crystallography: Chester, England, 2006; Vol. C.
- (37) *Solid State Physics*; Ashcroft, N. W., Mermin, N. D., Eds.; Holt, Rinehart and Winston: New York, 1976.
- (38) *Powder Diffraction: theory and practice*; Dinnebier, R. E., Billinge, S. J. L., Eds.; Royal Society of Chemistry: Cambridge, U.K., 2008.
- (39) Brent, R. P. *Algorithms for minimization without derivatives*; Prentice-Hall: New York, 1973.

JP108545Z